ARL-TR-9592 ● Oct 2022

DEVCOM ARMY RESEARCH LABORATORY

Low-Velocity Impact Performance of Indexed Fiber Architecture Ultra-High-Molecular-Weight Polyethylene Plates for Personnel Protection Systems

by Steven E Boyd

NOTICES

Disclaimers

The findings in this report are not to be construed as an official Department of the Army position unless so designated by other authorized documents.

Citation of manufacturer's or trade names does not constitute an official endorsement or approval of the use thereof.

Destroy this report when it is no longer needed. Do not return it to the originator.

ARL-TR-9592 ● OCT 2022

Low-Velocity Impact Performance of Indexed Fiber Architecture Ultra-High-Molecular-Weight Polyethylene Plates for Personnel Protection Systems

Steven E Boyd
DEVCOM Army Research Laboratory

REPORT DOCUMENTATION PAGE

Form Approved
OMB No. 0704-0188

1. REPORT DATE *(DD-MM-YYYY)*	2. REPORT TYPE	3. DATES COVERED (From - To)
October 2022	Technical Report	1 May 2021–26 August 2022

4. TITLE AND SUBTITLE
Low-Velocity Impact Performance of Indexed Fiber Architecture Ultra-High-Molecular-Weight Polyethylene Plates for Personnel Protection Systems

5a. CONTRACT NUMBER

5b. GRANT NUMBER

5c. PROGRAM ELEMENT NUMBER

6. AUTHOR(S)
Steven E Boyd

5d. PROJECT NUMBER

5e. TASK NUMBER

5f. WORK UNIT NUMBER

7. PERFORMING ORGANIZATION NAME(S) AND ADDRESS(ES)
DEVCOM Army Research Laboratory
ATTN: FCDD-RLW-MA
Aberdeen Proving Ground, MD 21005

8. PERFORMING ORGANIZATION REPORT NUMBER
ARL-TR-9592

9. SPONSORING/MONITORING AGENCY NAME(S) AND ADDRESS(ES)

10. SPONSOR/MONITOR'S ACRONYM(S)

11. SPONSOR/MONITOR'S REPORT NUMBER(S)

12. DISTRIBUTION/AVAILABILITY STATEMENT
Approved for public release: distribution unlimited.

13. SUPPLEMENTARY NOTES
ORCID ID: Steven E Boyd, 0000-0002-7554-8922

14. ABSTRACT

A flat plate low-velocity impact performance evaluation was conducted on four commercially available ballistic-grade ultra-high-molecular-weight polyethylene (UHMWPE) materials with three different fiber architectures (suggested by prior ballistic testing at the US Army Combat Capabilities Development Command Army Research Laboratory) and architecture configurations representative of those encountered in thermoformed complex double curvature structures. The four UHMWPE materials encompass a wide range of ballistic-grade materials to represent both fiber and film systems and compliant and stiff matrix binder materials. The three fiber architectures consisted of the reference (baseline) cross-ply architecture, a Helical –45 architecture (fully quasi-isotropic architecture with a periodicity of 2), and a 50%/50% combination of the two. The impact samples were evaluated at two impact energies, 50 and 70 J, which directly correlate to prescribed impact velocities defined under blunt impact conditions for combat helmets. The key screening metrics include dynamic peak back-face deflection, displacement contour at peak, and residual dent. The deformation and damage mechanisms per material per fiber architecture were also evaluated to identify the dominant mode of damage.

15. SUBJECT TERMS
ultra-high-molecular-weight polyethylene, UHMWPE, composites, low-velocity impact, LVI, fiber architecture, indexing, Mechanical Sciences, Sciences of Extreme Materials

16. SECURITY CLASSIFICATION OF:			17. LIMITATION OF ABSTRACT	18. NUMBER OF PAGES	19a. NAME OF RESPONSIBLE PERSON
a. REPORT	b. ABSTRACT	c. THIS PAGE			Steven E Boyd
Unclassified	Unclassified	Unclassified	UU	48	19b. TELEPHONE NUMBER (Include area code) (410) 306-1927

Contents

List of Figures

List of Tables

1. Introduction

The current state of the art (SoTA) in personnel armor protection systems uses ballistic-grade ultra-high-molecular-weight polyethylene (UHMWPE) composite materials due to their low specific density (approximately the same as water) and high tenacity of the fibrils that compose the fiber or film (tape) reinforcement phase. These UHMWPE materials are produced as unidirectional layers of aligned fibers or solid-state extruded films with a minimum of matrix material or coating for cohesion. Material manufacturers assemble these unidirectional layers into cross-ply orientations ($[0°/90°]_n$) of either two or four sublayers (Fig. 1), lightly consolidated with proprietary matrix materials to form flat cross-plied sheets of laminated UHMWPE composite materials to facilitate handling for manufacture and storage/shipping. Decades of ballistic impact testing on UHMWPE materials have demonstrated that the cross-plied fiber architecture performs in resistance to penetration (RTP) V_{50} limiting velocities testing and conforms well to the industry-standard matched metal tooling thermoforming (compression consolidation) process. Therefore, ballistic-grade, flat feedstock UHMWPE materials have evolved for direct application in armor systems that are lightweight, require a minimum ballistic performance against specified threats (specified RTP V_{50} and spall catching performance), and are easily thermoformed into structures with either mild curvature (torso armor plates) or complex double curvatures (a nearly hemispherical helmet shell).

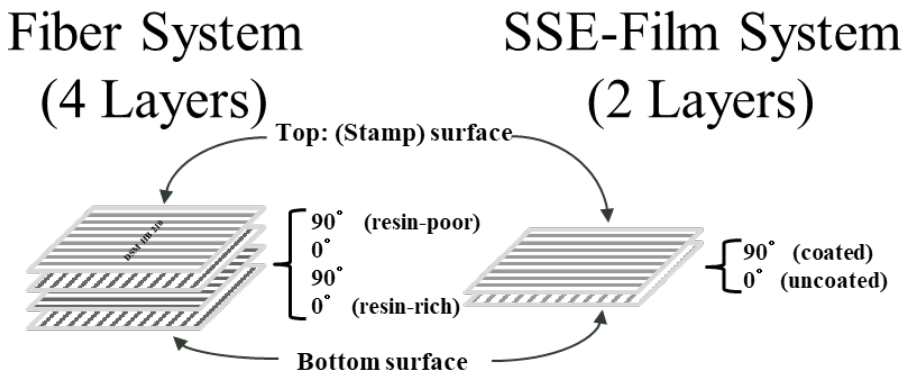

Fig. 1 Sublayer fiber architecture of commercially available UHMWPE laminated flat feedstock sheets

Cross-ply UHMWPE materials have enabled the design and manufacture of next-generation armor systems that achieve higher levels of ballistic threat resistance (RTP performance) than would be attainable with previous-generation aramid fiber composite materials. The key limiting characteristic of ballistic-grade UHMWPE materials is their set cross-plied material orientation, the design of which has solely

evolved to address ballistic threats. Although ballistic performance is paramount, the majority of warfighter injuries result from low-velocity impact (LVI) or blunt impact.[1,2] Both behind-helmet blunt trauma (BHBT) and behind-armor blunt trauma (BABT) are caused by excessive dynamic peak back-face deflection (BFD) under impact. The possibility for severe injury or death increases significantly when the armor deforms enough under impact that the offset distance is exceeded and the armor contacts either the head or torso, directly delivering a portion of the impact into the warfighter. Helmet shell-to-head contact is one of the chief causes of debilitating traumatic brain injuries.[3–5]

There are several mechanisms to stiffen UHMWPE material structures, mitigate excessive dynamic peak BFD, and limit armor-to-warfighter contact. The selection of material reinforcement (fiber, film, or fused-fiber), matrix binder (polyurethane [PU], polyethylene [PE], or polyolefin coating), and a proprietary tailoring of fiber sizing/interface chemistry can all be utilized to stiffen a UHMWPE laminate plate under impact and achieve decreased dynamic peak BFD in out of plane flexure. A previous research effort detailed the evaluation of a variety of ballistic-grade UHMWPE materials subject to LVI at multiple energies[6] and concluded notable performance differences (peak contour, peak BFD, etc.) with just cross-ply fiber architectures. Another way of stiffening the flexure of UHMWPE material plates under impact is through tailoring fiber architectures. Basic mechanics of laminated composite materials, such as classical laminated plate theory, demonstrate that a cross-ply fiber architecture is highly orthogonal with high effective laminate stiffness only in the 0° and 90° orientation. Incorporating discrete bias offset angles such as 22.5°, 30°, 45°, and 60° into the lay-up changes the laminate properties from a cross-ply to a more quasi-isotropic in-plane symmetry for the laminate properties. The only way of introducing bias angles into a laminate fabricated with as-manufactured cross-plied UHMWPE sheets is through indexing individual sheets by a discrete bias angle, thus creating layers that have the orientations of [22.5°/112.5°], [30°/120°], [45°/135°], and [60°/150°] (or any orthogonal angle combination).

Other researchers have investigated the effects of offset angle fiber architectures on the impact performance of flat UHMWPE material plates. Researchers at the US Army Combat Capabilities Development Command (DEVCOM) Army Research Laboratory (Vargas-Gonzalez et al.[7–9]) proposed what is now known as the legacy "ARL X-hybrid" fiber architecture, which features a 75% target areal density (AD; selected here to be 11.7 kg/m^2) conventional cross-ply strike face with a 25% AD back face composed of helical indexing of every other layer by 22.5°. They conducted RTP testing with various projectiles and found that this fiber architecture configuration achieved a 40% decrease in dynamic peak BFD compared to the

reference 100% AD cross-ply panel with no reduction of RTP properties (i.e., no drop in V_{50}). The ARL X-hybrid configuration was further extended to offset angles of 30° and 45° for ease of fabrication and to limit material waste. The research also evaluated the impact performance of the "helical" or "helicoid" laminates composed of 100% AD helical indexing (again at 22.5°, 30°, and 45°) and found that these laminates exhibited the lowest dynamic peak BFDs and deformation profiles, although with an 8%–11% decrease in RTP limiting velocity (V_{50}). There was a statistically negligible difference in the peak BFD versus RTP performance with the 30° and 45° indexed laminates.

Hazzard et al.[10] investigated the effect of fiber architecture on the LVI performance of flat UHMWPE plates consisting of offset angles (45°, 22.5°, 11.25°, and 5.6°) to construct helicoidal architectures to form a laminate through indexing cross-plied sheets. Panels (specified as lay-ups only with no target AD) were center impacted at 150 J with clamped boundary conditions, and the BFD field was measured with stereo high-speed imaging and correlated with digital image correlation (DIC; 3-D or stereo). A 50% reduction in the maximum BFD was observed for the quasi-isotropic and three helicoid architectures versus the reference cross-ply architecture; however, there was negligible performance difference (all had similar dynamic peak BFDs) between the quasi-isotropic and helicoid architectures, suggesting that the more fabrication-efficient quasi-isotropic architecture (with [45°/135°] sheets) achieved a similar performance objective.

This brief literature survey demonstrates that even a small percentage (by AD) of bias offset angle plies (especially [45°/135°]) introduced into the reference cross-ply lay-up can significantly reduce dynamic peak BFD while having a negligible impact on RTP performance (V_{50}). This trend is observed and reported across the impact velocity regime (from LVI[10] to ballistic limit[7–9]) and is representative of variety of ballistic-grade UHMWPE material systems. However, displacing too many [0°/90°] sheets (plies) presents a trade space decision point where minimizing peak BFD must be balanced with maintaining threshold RTP performance (V_{50}) and must align with the intended application.

The goal of the current research is to investigate the beneficial effects of fiber architecture and evaluate inclusion into personnel protection systems. A previous effort presented a flat UHMWPE LVI methodology[6] designed to directly correlate to the blunt impact rating criteria for UHMWPE helmet shells and modeling component to extract high-confidence material properties.[11] The research presented experimental characterization of SoTA ballistic-grade UHMWPE materials subject to LVI at several impact energies but was limited to the cross-ply fiber architecture. That approach is extended in this research to evaluate fiber architectures based on the legacy ARL X-hybrid and helical configurations with a downselection of

representative ballistic-grade UHMWPE material systems relevant to personnel protection systems. This research can also be used to propose UHMWPE materials and fiber architectures for mild curvature personnel protection systems like torso protection plates.

Four SoTA ballistic-grade UHMWPE material systems with a variety of fiber reinforcements and matrix materials are subject to flat plate LVI at two impact energies corresponding to blunt impact criteria for UHMWPE helmet shells.[6] The target AD was 11.7 kg/m^2. Three fiber architectures are investigated, including the previously evaluated cross-ply architecture and two new architectures incorporating a "helical" design with a single bias offset angle (45°). These alternate fiber architectures are created by indexing cross-plied sheets of flat UHMWPE feedstock material (off the roll) within the lay-up and did not use the more difficult to handle unidirectional sublayers. Two replicate impacts are conducted for most of the materials subject to material availability. The BFD field is recorded during the impact event using high-speed imaging and stereo DIC to determine the dynamic peak BFD and displacement contour at peak BFD. Deformation and damage mechanisms are visualized using X-ray computed tomography (XCT) with a particular interest in through thickness damage mechanisms such as delamination, fiber pull-out and kinking, and visualizing the interface of dissimilar fiber architectures.

2. Materials and Processing

2.1 Materials

A detailed discussion of the UHMWPE material systems selected for testing and their individual processing schedules (including modifications) is given in Boyd.[6] Four of those materials are downselected for the present fiber architecture study and presented in Table 1. The four selected UHMWPE material systems comprise three commercially available fiber/matrix systems and one solid-state extruded (SSE) film/coating system. These materials represent leading candidates for inclusion in personnel protection systems and include DSM Dyneema HB210 and HB212, Honeywell SpectraShield (SS) 4232, and Du Pont Tensylon HSBD 30A. The DSM materials have the same AD and differ only by matrix material. The Tensylon film system has the lowest AD and is the thinnest material feedstock sheet, requiring over 100 layers to achieve the target AD. The Honeywell SS-4232 is the thickest material with the highest AD. All panels were fabricated with a target AD of 11.7 kg/m^2. DSM Dyneema HB212 has a rubber-based polymer matrix making it the most compliant of the group. Du Pont Tensylon HSBD 30A is an SSE-film system that is both thin and very stiff making it less suitable for

thermoforming of complex double curvature structures but a potentially excellent choice for flat and mild curvature plates. Tensylon also has the lowest matrix volume content of the UHMWPE materials in this study. The remaining two materials, DSM Dyneema HB210 and Honeywell SpectraShield 4232, are both fiber/matrix systems with a good combination of stiff UHMWPE fibers and PU matrices, giving them good RTP and structural performance.

Table 1 SoTA UHMWPE composite materials used in this fiber architecture study

Materials		Manufacturer AD (single layer) (g/m^2)	No. of plies target AD (11.7 kg/m^2)	Reinforcement system (orthogonal)	Matrix material
DSM Dyneema	HB210	136 ± 5	87	Fiber	PU rubber-based Polymer Polyolefin coating PU
	HB212	136 ± 5	87	Fiber	
DuPont Tensylon HSBD	T30A	111 ± 7	106	SSE-film	
Honeywell SpectraShield	SS-4232	168	70	Fiber	

2.2 Fiber Architecture

All fiber/matrix systems consist of four orthogonal sublayers of [0°/90°/0°/90°] plies in an as-manufactured flat feedstock sheet as diagramed in Fig. 1 (left side). The Tensylon 30A SSE-film system is thinner consisting of only two orthogonal sublayers of [0°/90°] (Fig. 1, right side). The manufacturer's branding side is resin-poor (duller appearance) with the opposite side being resin-rich (shiny) to promote good bonding of stacked layers during compression consolidation at temperature. As stated, the evolution of this cross-plied flat feedstock material was motivated by ballistic performance and ease of handling and storage as the unidirectional sublayers are very difficult to handle and fabricate into a panel. The cross-ply architecture of the fiber/matrix systems also exhibit good in-plane shearing, making them amenable to thermoforming complex curvature structures.

There are two ways to introduce bias offset angle fiber architectures into ballistic-grade UHMWPE material laminates. First, unidirectional sublayers can be acquired through special order and agreement with the material manufacturer, or the commercial cross-plied product can be indexed by a discrete angle, as illustrated in Fig. 2. Some researchers have investigated the impact performance of UHMWPE laminates using the unidirectional sublayer (single-layer sheet) as a building block[12] to create genuine quasi-isotropic and helicoidal fiber architectures without any orthogonal interfaces (i.e., a discontinuous transition between two orthogonal layers). The processing difficulty of handling and fabricating a panel with unidirectional materials as building layers is warranted for research focused on the impact performance of sheared fiber architectures that arise from extensive in-plane

shearing when thermoforming complex double curvature structures. For this research, it proved sufficient to use indexed cross-plied UHMWPE material sheets to introduce quasi-isotropic symmetry fiber architectures. Indexing of cross-plied UHMWPE feedstock sheets create laminates that exhibit uniform effective laminate properties and retain the orthogonal interfaces, which are both thermoformable and demonstrate excellent RTP performance.

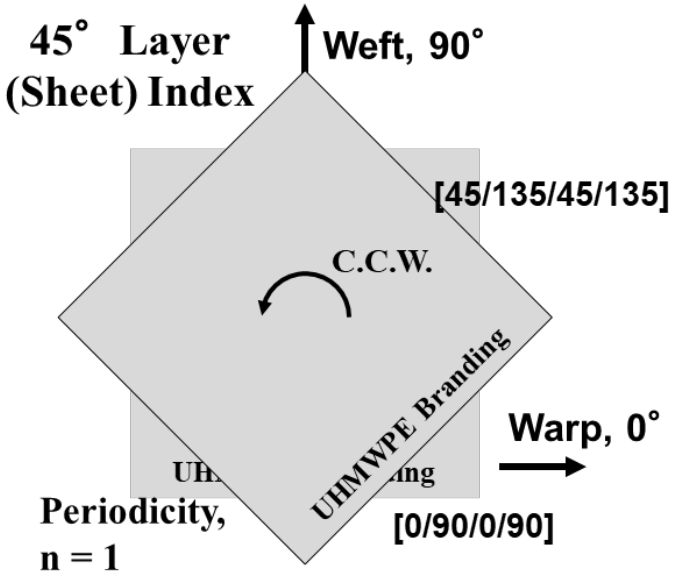

Fig. 2 Illustration of the concept of indexing cross-plied UHMWPE flat feedstock sheets. The lay-up is defined by the bias offset angle (45° is pictured) and the periodicity (rotation frequency). A periodicity of n = 1 represents alternating every layer.

Vargas-Gonzalez et al.[9] addressed several issues related to indexing cross-plied layers, including offset angle (22.5°, 30°, or 45°) and periodicity of indexing (i.e., indexing every layer vs. indexing after ***n*** number of layers). All offset angles performed well versus the reference cross-ply architecture, where good performance was defined as a careful balance of minimizing peak BFD while maintaining RTP V_{50}. Although the legacy ARL X-hybrid 22.5° offset angle demonstrated a better RTP V_{50}, the 30° and 45° only saw a 5% and 7% drop, respectively; all offset angles had statistically similar peak BFDs. Periodicities of ***n*** = 1, 2 were investigated, but only for the legacy ARL X-hybrid fiber architecture (22.5°). The effect of periodicity (rotation frequency) is illustrated on a hypothetical 20-ply laminate whose lay-up is represented in Appendix A, Fig. A-1. A less than 10% improvement in the dynamic peak BFD and 10% drop in the RTP V_{50} for the higher periodicity, ***n*** = 1, was observed. A review of the results presented in Vargas-Gonzalez et al. revealed fiber architecture parameters and a periodicity to focus on for the current research. Three fiber architectures were selected, as illustrated in Fig. 3: the reference (baseline) cross-ply (CP), a helicoid ("Helical – 45") with an

offset angle of 45°, and a combination of both like the proposed ARL X-hybrid (again with 45° offset angle and referenced as either "ARL X-hybrid – 45" or "CP/Helical – 45"). The 45° offset angle was selected because the trade space performance of peak BFD versus RTP V_{50} was statistically equivalent to the other acute angles investigated and 45° sheets are easier to cut in a diamond pattern, which results in cost savings and less waste of ballistic-grade UHMWPE material. A periodicity of $\boldsymbol{n}$ = 2 was selected based on the results presented by Vargas-Gonzalez et al.[9] A weighting of CP to helical—45 of 50% to 50%—was selected to introduce more [45°/135°] layers into the laminate in hopes of guaranteeing an observable performance difference. A polar plot of the effective laminate stiffness of all three fiber architectures is given in Fig. 4 demonstrating the beneficial effect of introducing 45° indexed layers into highly orthogonal laminates.

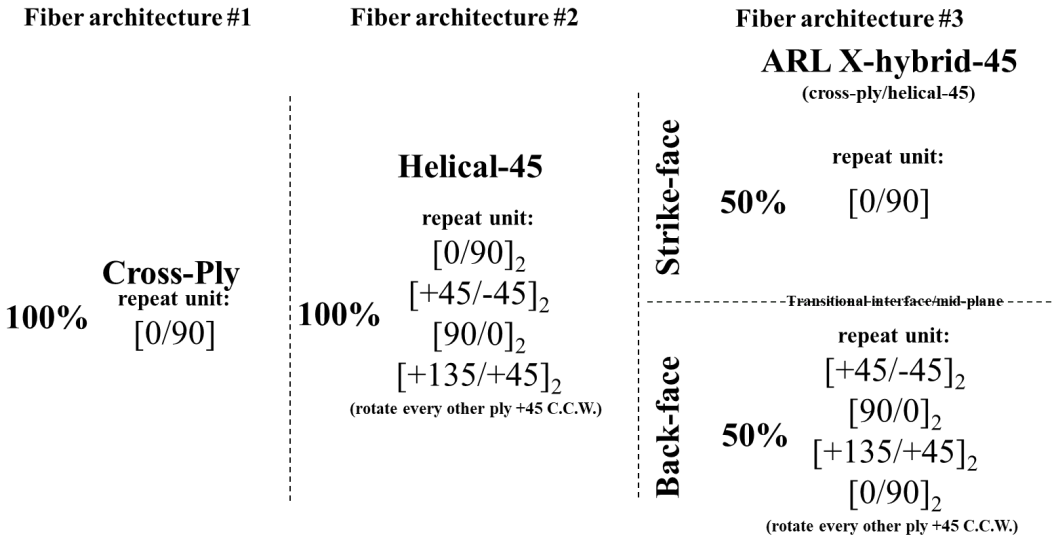

Fig. 3 Laminate lay-ups (with repeat units until the target AD is achieved) for all three fiber architectures evaluated in this study: 100% CP and 100% Helical – 45 and a split combination of both with the CP orientation on the strike face. The periodicity is n = 2 with every other ply rotated with respect to the warp or 0° (direction of the stamp or branding).

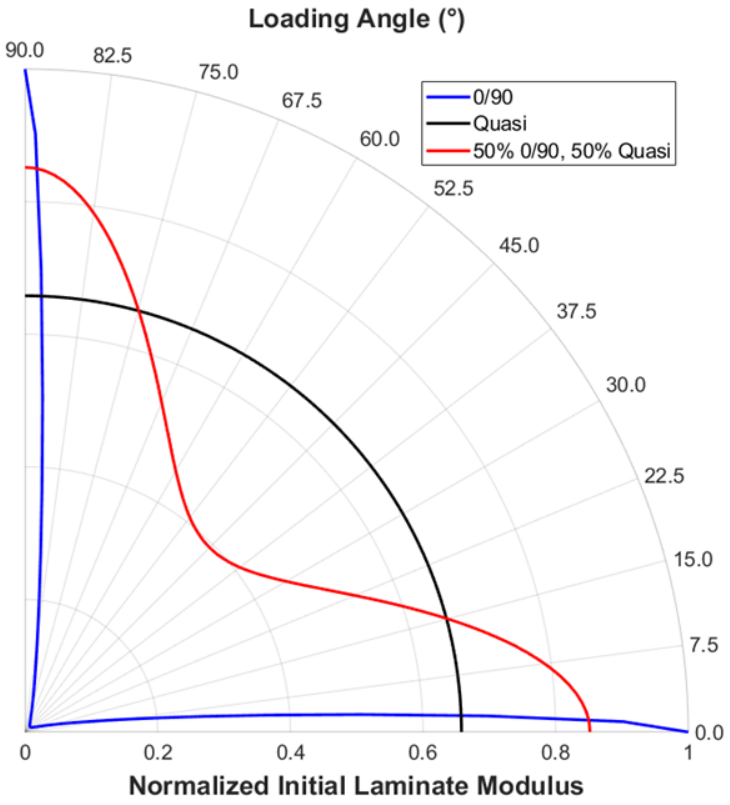

Fig. 4 Polar plot of normalized effective laminate stiffness vs. loading angle calculated from classical laminated plate theory and laminate fiber orientation for a ballistic-grade UHMWPE material. The orthogonal CP fiber architecture is very stiff in the 0° and 90° but negligible in between (blue line). The Helical – 45 or quasi-isotropic laminate has a uniform stiffness invariant of loading angle (black line). A 50%/50% combination of both (red line) demonstrates a "softer" fluctuation in stiffness.

2.3 Impact Sample Preparation

All panels were fabricated and processed as detailed in Boyd.[6] A large 45.7-cm-square panel with a target AD of 11.7 kg/m^2 was manufactured for each material and each fiber architecture (the CP panels were manufactured and tested previously). Several parent panels were manufactured for replicate testing. A micro waterjet (MicroMax, OMAX Corporation) cut five to nine impact samples out of each panel to final dimensions of 15.2 cm × 15.2 cm × 1.3 cm. The manufacturer's branding or stamp side was consistently used as the LVI strike face, except for the X-hybrid architecture (CP/Helical – 45), which was impacted on both sides to examine the effects of sequencing (i.e., CP/Helical – 45 vs. Helical – 45/CP) on the impact response. Each impact sample was labeled and speckled on the back face with a flat white background and a flat black medium speckle pattern for stereo high-speed imaging and DIC during the impact event.

2.4 Drop Tower Impact Testing and Displacement Measurement

A detailed description of the drop tower experimental configuration and high-speed imaging data acquisition and DIC analysis is given in Boyd.[6] All 15.2 cm × 15.2 cm × 1.27 cm impact samples were impacted with a 50.8-mm-diameter hemispherical impactor. For this study, the 25-J impact energy was dropped in favor of the 50- and 70-J impact energies to render the testing matrix more manageable. The 50-J impact corresponds to a 5.5-kg drop carriage with a drop height of 93 cm and the 70-J impact to a 7-kg carriage dropped at 1.1 m. Two energies proved to be sufficient to provide a picture of the impact response as well as calibrate and validate the modeling component in Staniszewski et al.[11] The square impact samples were confined in a simply supported fixture, as pictured in Fig. 5. The support rails provide a square footprint support condition, which is important given that multiple fiber architectures were now being tested under axisymmetric LVI loading. A quick computational assessment was undertaken to quantify the effect of the square support conditions versus a circular (annulus) support (see Figs. 5 and 6 in Boyd[6]) on the two fiber architectures that contain a large fraction of [45°/135°] layers. The simulations comparing support geometries demonstrated only a 1.8% and 3.5% difference in the predicted peak BFD for the CP and Helical – 45 fiber architectures, respectively. As a result, a decision was made to keep using the LVI fixture with the square supports to be consistent with Boyd.[6] No adjustment was made to the stereo high-speed imaging configuration and DIC analysis from Boyd.[6]

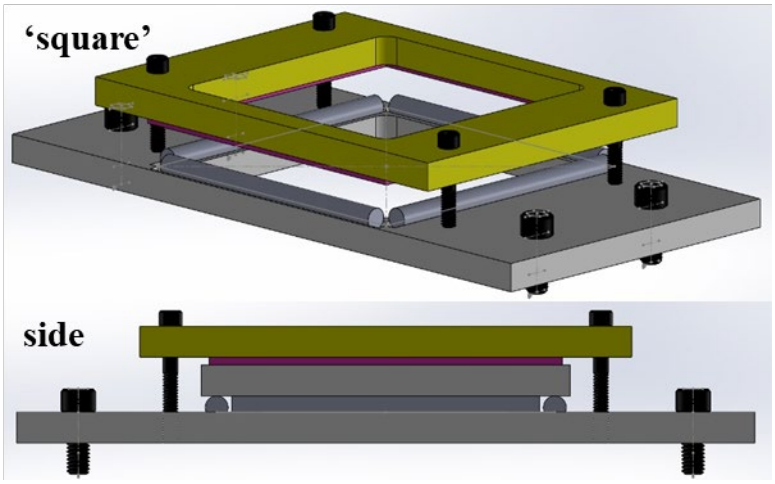

Fig. 5 Impact test fixture for drop tower impact testing illustrating "square" simply supported boundary conditions without impact sample (top) and side view with impact sample (bottom)

The 3-D DIC gave the BFD field including the dynamic peak BFD profile, the deformation contour, and an estimate of the post-transient displacement, which is

effectively the permanent dent at the point of impact. The instantaneous impact force in the instrumented impactor was recorded and synced with the high-speed imaging and used to provide a validation for the DIC measured peak BFD profile. Replicate tests were performed for the DSM Dyneema HB210 and HB212 materials, but not for the Honeywell SS-4232 and Tensylon 30A.

2.5 Post-Impact Deformation Analysis

After the samples were impacted, two nondestructive techniques were used to visualize the deformation and internal damage. All sample strike faces were photographed using bright light sources (the same used to illuminate the back face during the impact event) and a digital high-definition camera. Because of the translucent property of UHMWPE composites, visualization with a bright light source can reveal the extent of the external dent with more clarity and hint at the internal damage area including kink-band formation (appearing like dark lines), which may extend to the edge following the fiber orientation. For this study, ultrasonic C-scan techniques were omitted in favor of more detailed XCT imaging.

Most post-impact samples were scanned in groups of three or four using a North Star X5000 (North Star Imaging). The scans were analyzed in an open-source program called 3DSlicer (Harvard Medical School), which was run within the Department of Defense High-Performance Computing Modernization Program environment. A few of the samples were analyzed on a desktop computer using Bruker's proprietary software CT-Vox. The XCT data was reduced to a set of 2-D images along all three axes for the impacted samples (X, Y, and Z [through-thickness]) and analyzed to assess the deformation and damage mechanisms.

3. Results and Discussion

The LVI performance results and follow-up discussion are presented per material. The effect of fiber architecture on LVI performance is summarized through a discussion of the peak dynamic BFD, the displacement contour at peak, and XCT imaging of deformation and damage due to impact. These three metrics are correlated with the material system, impact flexural mechanics, interface discontinuities related to layer orthogonal fiber architectures, and fiber architecture sequence effects. This study employs the flat plate LVI characterization methodology developed in Boyd[6] and modeled in Staniszewski et al.[11] and is therefore limited to low-velocity regime impacts. The characterization methodology is designed to directly correlate to blunt impact scenarios in combat helmet shells manufactured with ballistic-grade UHMWPE materials and provides a durability and screening metric for evaluating materials for personnel protection

systems. The reviewed literature suggests that the beneficial influence of fiber architecture over impact response demonstrates trends that are observable in both LVI and ballistic impact regimes. The goal of this study is to better understand how fiber architecture affects the impact response (displacement–time profile and displacement contour) and influences the deformation and damage mechanics. This provides an understanding of how to tailor and incorporate the beneficial structural mechanics of fiber architectures into personnel protection systems such as combat helmets and torso plates.

3.1 LVI Response of DSM Dyneema HB212

The correlation results for the peak dynamic BFD and residual dent (post-transient impact event) are summarized for DSM Dyneema HB212 in Table 2. Table 2 presents the peak BFD and impact efficiency at two impact energies, 50 and 70 J. The 25-J impact energy data is stated for the CP fiber architecture only to represent previous impact work[6] for completeness and comparison. The impact efficiency is defined as the ratio of residual dent divided by peak BFD at the impact site. Figure 6 provides a convenient graphical summary of the peak dynamic BFD for HB212 for all fiber architectures. Provided error bars reflect the standard deviation (STD) for the peak BFD for at least two replicate impact tests. The 50-J impact for the CP architecture is the only test to have a replicate due to the excessive peak BFD encountered (18.4 mm). Because of this excessive BFD at 50 J, a 70-J test was not attempted for the CP architecture due to concerns with the DIC correlation accuracy (excessive out-of-focal plane deflections) and the risk of punching the compliant HB212 through (off) the square supports. Finally, impact samples labeled CP/Helical – 45 and Helical – 45/CP were cut from the same parent panel and were impacted on opposite sides (i.e., the strike face was either the CP or Helical – 45 side).

Table 2 Peak dynamic BFD measured through DIC for DSM Dyneema HB212 per fiber architecture for each impact energy

DSM HB 212	Impact energy					
	25 J		50 J		70 J	
	Peak δ (mm)	Impact efficiency	Peak δ (mm)	Impact efficiency	Peak δ (mm)	Impact efficiency
CP	11.6	0.14	18.4 ± 0.6	0.14 ± 0.01	N/A	N/A
CP/Helical – 45	N/A	N/A	10.4 ± 1.0	0.29 ± 0.01	13.4 ± 1.1	0.33 ± 0.03
Helical – 45/CP	N/A	N/A	11.2 ± 0.8	0.36 ± 0.05	13.7 ± 1.0	0.36 ± 0.07
Helical – 45	N/A	N/A	10.3 ± 0.2	0.27 ± 0.01	12.6 ± 0.7	0.32 ± 0.01

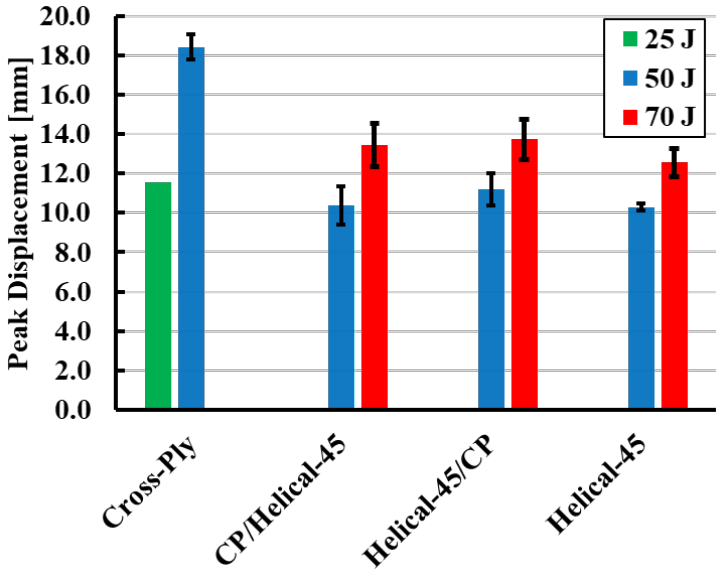

Fig. 6 Peak BFD for DSM Dyneema HB212 for each fiber architecture at impact energies of 25, 50, and 70 J

The relatively large BFDs presented in Table 1 and Fig. 6 are expected with the HB212 as it is specifically engineered with a compliant rubber-based polymer matrix to increase the mechanism of impact energy dissipation through large flexural deflections for CP fiber architectures. Even though HB212 has a compliant rubber-based polymer matrix, adding approximately 25% by AD [45°/135°] plies post a 44% and 39% decrease in the peak BFD for the CP/Helical – 45 and Helical – 45/CP architectures, respectively, in the 50-J impact case. This is a significant improvement in flexural rigidity under impact for this compliant material. For the 100% Helical – 45 architecture, which displaces 50% of the [0°/90°] plies in the CP/Helical – 45 case with [45°/135°], no further improvement is seen (still a 44% decrease in peak BFD). This strongly suggests that "loadings" of [45°/135°] plies need only be 25% (or possibly less, as investigated by Vargas-Gonzalez et al.[9]) to improve the structural impact performance of structures containing HB212. Again, to maintain the RTP V_{50} performance of these ballistic-grade UHMWPE materials, displacing as few [0°/90°] plies as possible is preferred.

For HB212, there is a slight improvement (–5%) in the average peak BFD with sequencing of the fiber architectures of 44% for CP/Helical – 45 versus 39% for Helical – 45/CP. This improvement is also represented in the impact efficiency at 50 and 70 J in Table 2. When an impact sample is struck, the strike face goes into dynamic flexural compression and the back-face flexural tension. It is postulated (or expected) that the stiffer fiber architecture, which is the Helical – 45 (closer to a quasi-isotropic architecture as demonstrated in Fig. 4), would improve the impact performance (post a reduced peak BFD) when configured on the back face (the

material configuration investigated by Vargas-Gonzalez et al.[9]). However, the indicated 5% improvement is statistically indeterminate due to the standard deviation (approximately 1 mm of deflection) between the impact test replicates and no firm benefit of preferentially sequencing CP/quasi-isotropic architectures could be identified. The 100% Helical – 45 architecture posted the lowest peak BFD, but it was not statistically better than the CP/Helical – 45 architecture, suggesting the investment of the extra [45°/135°] plies had no additive effect.

The displacement contours of HB212 at peak BFD for 50- and 70-J impact energies are given in Figs. 7 and 8, respectively. A single replicate is posted for the different fiber architectures except two are shown for the cross-ply 50-J impact. The stated 44% drop in peak BFD between the cross-ply architecture (green curve) and the remaining architectures containing [45°/135°] plies (blue, red, and black curves) is starkly represented in Fig. 7. There is also a discernable difference in the shape of the contour at peak between the cross-ply fiber architecture and the architectures containing [45°/135°] plies. The green curve in Fig. 7 has more of a rounded bell shape versus a flatter triangular shape represented by the 100% Helical – 45 (black curve). This shape could be attributable to the fiber tension pull-out along the reinforcement directions (0° and 90°) hinted at in Appendix B, Fig. B-1 (visualization of strike face for HB212), which prominently show a “square” framing of the vicinity of the impact site that disappears as more [45°/135°] plies are added in (transitioning the architecture from fully CP to quasi-isotropic). Again, the displacement curves for the sequenced fiber architectures, CP/Helical – 45 and Helical – 45/CP, are very similar with the curves at 70 J in Fig. 8 where they are nearly overlapping. The 100% Helical – 45 curves, as expected, have the lowest peak BFD.

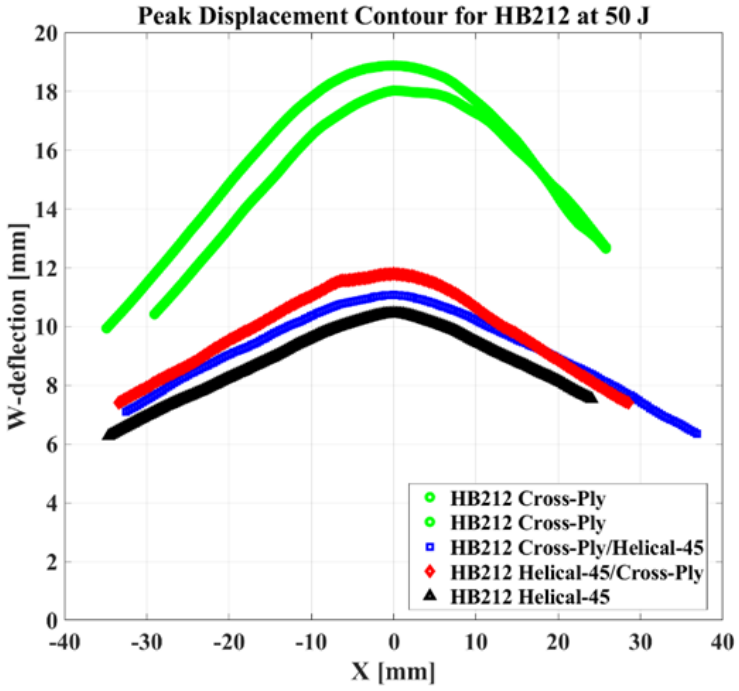

Fig. 7 Displacement contour at peak BFD for a 50-J impact energy for DSM Dyneema HB212

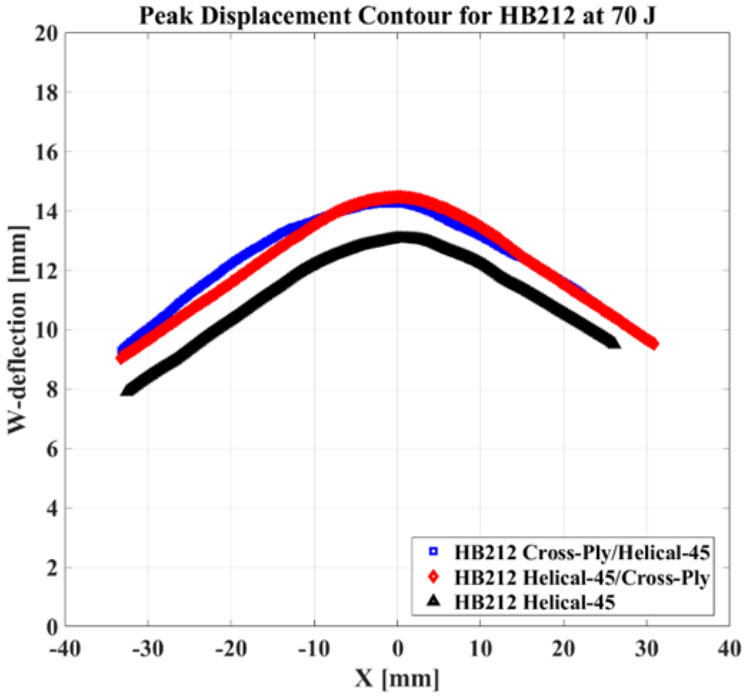

Fig. 8 Displacement contour at peak BFD for a 70-J impact energy for DSM Dyneema HB212

3.2 LVI Response of DSM Dyneema HB210

The DIC results for the dynamic peak BFD for DSM Dyneema HB210 are stated in Table 3 and graphically summarized in Fig. 9. The HB210 is the stiffer of the two DSM Dyneema materials with a PU matrix and, perhaps, a proprietary sizing component to promote bonding and structural stiffness. The trends observed with HB212 are again demonstrated with HB210 but with a more modest drop in BFD for the stiffer material. The 100% Helical – 45 fiber architecture posts the best peak BFD with a 23% and 26% decrease over the reference CP architecture for the 50- and 70-J impacts, respectively. The CP/Helical – 45 architecture also demonstrates a similar decrease in peak BFD with 16% and 21%, respective of impact energy. With the stiffer HB210 material, there is more support for preferential sequencing of the cross-ply and quasi-isotropic architectures, especially at the higher 70-J impact energy. At 70 J, the CP/Helical – 45 and Helical – 45/CP architectures post a 21% and 12% decrease in peak BFD for a net gain of 9% when the stiffer quasi-isotropic architecture is placed on the flexural tension back face. This may suggest that, for stiffer UHMWPE material systems, the effect of a stiffer versus more compliant laminate fiber architecture may act to counter global flexure under impact and beneficially stiffen the system solely through targeted fiber architecture placement through-thickness. For the HB210 material, the standard deviations in BFD between replicate impact tests are much tighter (only up to 0.3 mm from Table 3) supporting interpretation of this preferential sequencing trend.

Table 3 Peak dynamic BFD measured through DIC for DSM Dyneema HB210 per fiber architecture for each impact energy

DSM HB 210	Impact energy					
	25 J		50 J		70 J	
	Peak δ (mm)	Impact efficiency	Peak δ (mm)	Impact efficiency	Peak δ (mm)	Impact efficiency
CP	4.4	0.27	7.2	0.33	9.1	0.35
CP/Helical – 45	N/A	N/A	6.0 ± 0.1	0.29 ± 0.02	7.2 ± 0.1	0.31 ± 0.01
Helical – 45/CP	N/A	N/A	6.2 ± 0.2	0.32 ± 0.00	8.0 ± 0.2	0.38 ± 0.01
Helical – 45	N/A	N/A	5.5 ± 0.3	0.31 ± 0.03	6.8 ± 0.0	0.36 ± 0.01

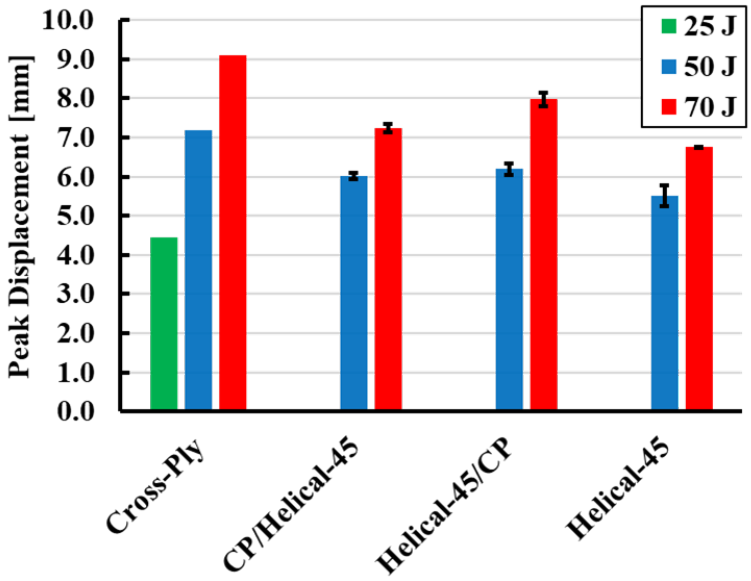

Fig. 9 Peak BFD for DSM Dyneema HB210 for each fiber architecture at impact energies of 25, 50, and 70 J

The displacement contours at peak BFD for DSM Dyneema HB210 at impact energies of 50 and 70 J is given in Figs. 10 and 11. The displacement contours at both impact energies display a bell shape for the CP fiber architecture and a more linear triangular for fiber architectures containing an increasing number of [45°/135°] plies. Also, the trend of decreasing peak BFD is observed at both impact energies transitioning from 100% CP to 100% Helical – 45 (quasi-isotropic) fiber architectures. The cross-ply and Helical – 45 fiber architectures display a 7% versus 5% drop in peak BFD at 50 and 70 J, respectively. The effect of sequencing fiber architectures is statistically inconclusive for the 50-J impacts as there is only a 2% difference in peak BFD between the CP/Helical – 45 and Helical – 45/CP fiber architectures. In contrast, at an impact of 70 J, the sequencing effect exhibits a more definitive difference in the CP/Helical – 45 and Helical – 45/CP fiber architectures, clearly differentiated in Fig. 11 (red vs. blue curve). This –9% improvement in the peak BFD is important because it suggests that, for higher impact energies, it may be more important to configure the globally stiffer quasi-isotropic fiber architecture on the back face, an experimental configuration selected by design for investigation by Vargas-Gonzalez et al.[9] Unfortunately, no ballistic evaluation of a reverse legacy ARL X-hybrid fiber architecture configuration was performed by Vargas-Gonzalez et al. to lend support for this conjecture. Investigating this type of sequencing effect on the impact response (both LVI and ballistic impact) is critically relevant to personnel protection systems as sequencing of CP and sheared architectures are known to occur in complex double curvature structures composed of ballistic-grade UHMWPE materials due to the thermoforming process.

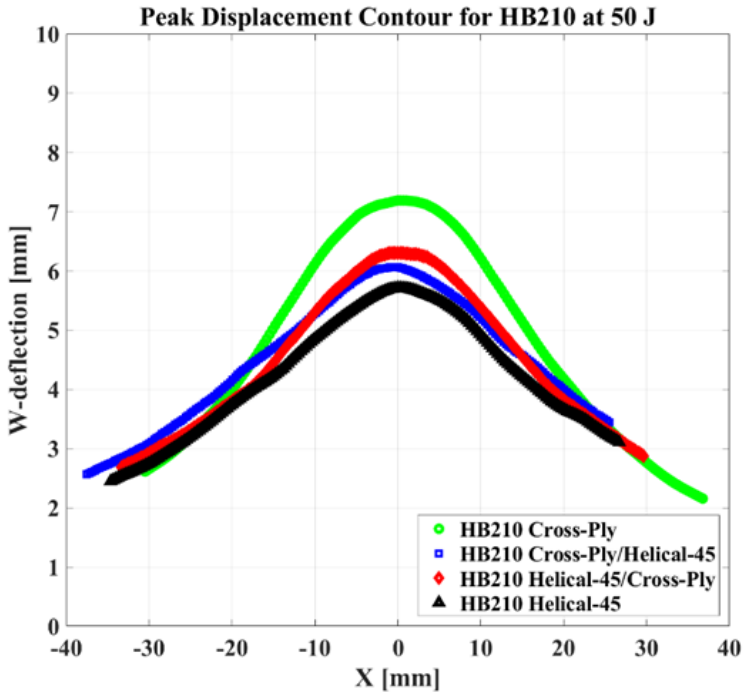

Fig. 10 Displacement contour at peak BFD for a 50-J impact energy for DSM Dyneema HB210

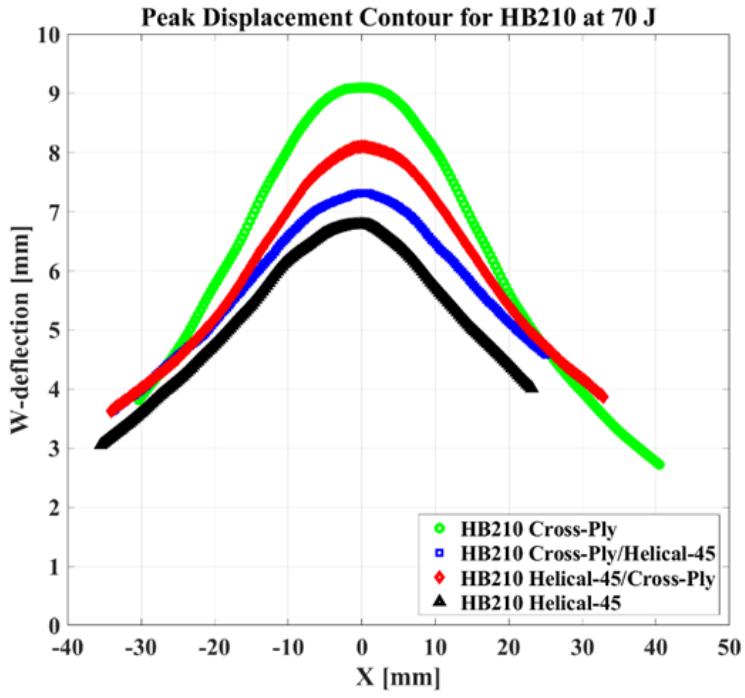

Fig. 11 Displacement contour at peak BFD for a 70-J impact energy for DSM Dyneema HB210

3.3 LVI Response of Du Pont Tensylon HSBD 30A

The DIC results for the dynamic peak BFD for Tensylon 30A are listed in Table 4 and graphically summarized in Fig. 12. Replicate testing was not performed for the Tensylon 30A material due to limited material availability during the time window of panel manufacture. Also, preliminary analysis of the LVI performance of HB210 indicated that the LVI performance of stiff UHMWPE materials has a high degree of reproducibility with minimum statistical scatter. The peak BFD data presented in Table 4 and Fig. 12 illustrates that the Tensylon 30A material system is very structurally stiff under impact at both impact energies of 50 and 70 J. At 50 J, the Tensylon 30A is not very sensitive to the effects of fiber architecture with a demonstrated drop in peak BFD of only 13% between the reference CP and Helical – 45 fiber architectures. This 13% drop in peak BFD may be grounded in the fact that this observed decrease occurs only over a range of approximately 1 mm of deflection. The limiting confidence of the high-speed imaging and DIC system is approximately 0.1 mm and the HB210 material has demonstrated a statistical variation of ±0.3 mm through replicate testing. Considering this, the 50-J impact energy may be too low to solicit an adequate impact response to evaluate trends in the impact performance for stiffer UHMWPE material systems as all the curves in Fig. 13 nearly overlap. The 50-J impact energy was selected for evaluation with all UHMWPE materials because it corresponds threshold criteria for blunt impact on a helmet shell.[13,14]

Table 4 Peak dynamic BFD measured through DIC for Du Pont HSBD Tensylon 30A per fiber architecture for each impact energy

Tensylon 30A	Impact energy					
	25 J		50 J		70 J	
	Peak δ (mm)	Impact efficiency	Peak δ (mm)	Impact efficiency	Peak δ (mm)	Impact efficiency
CP	4.0	0.25	6.0	0.34	7.7	0.41
CP/Helical – 45	N/A	N/A	5.6	0.33	6.6	0.37
Helical – 45/CP	N/A	N/A	5.8	0.34	7.6	0.38
Helical – 45	N/A	N/A	5.2	0.28	6.3	0.35

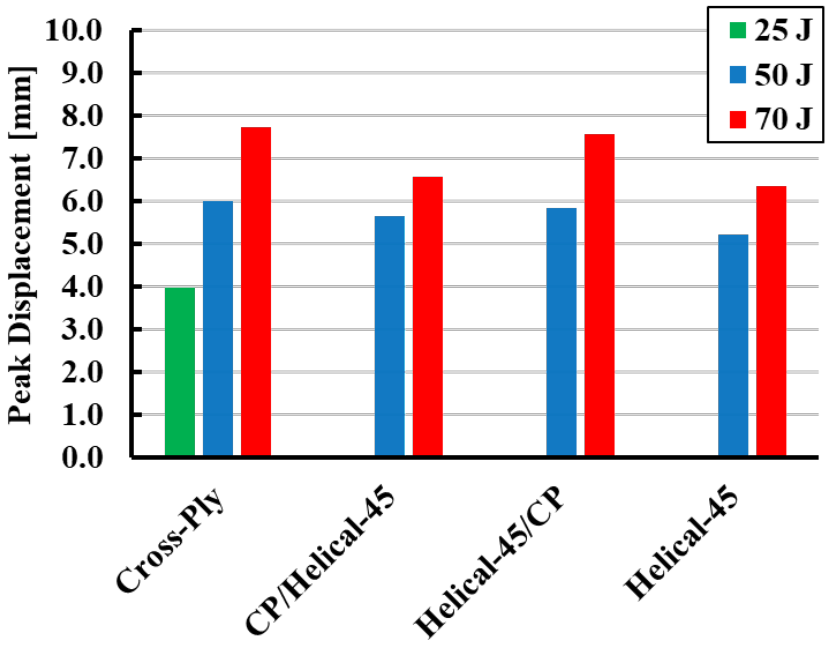

Fig. 12 Peak BFD for Du Pont HSBD Tensylon 30A for each fiber architecture at impact energies of 25, 50, and 70 J

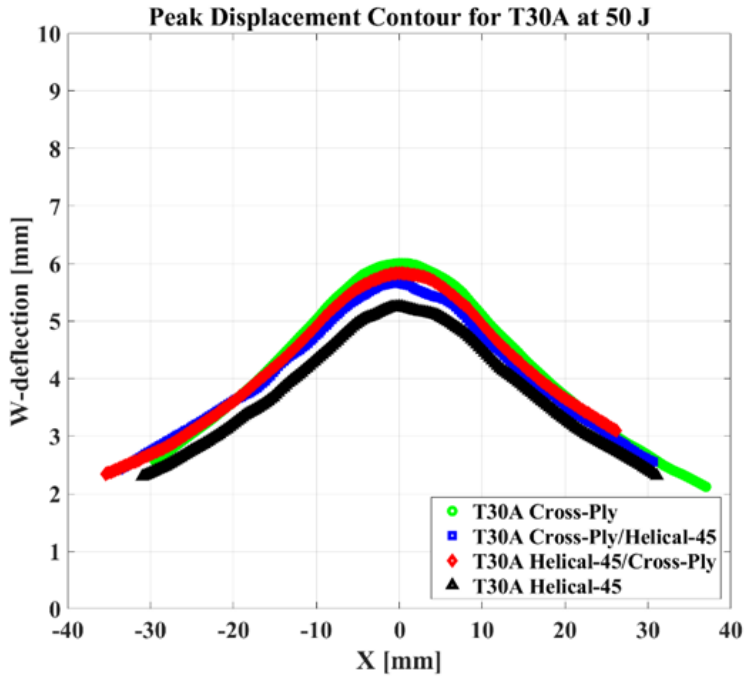

Fig. 13 Displacement contour at peak BFD for a 50-J impact energy for Du Pont HSBD Tensylon 30A

At an impact energy of 70 J, the decrease in the peak BFD is 15% between the reference CP and the CP/Helical – 45 architectures. This notable drop in peak BFD at higher impact energies achieved through adding as little as 25% AD of

[45°/135°] plies to the laminate lay-up is supported by impact data from HB212 and HB210. Interestingly, the Helical – 45/CP fiber architecture performs no better than the reference CP with a small –2% decrease in peak BFD. This suggests that the material morphology of the reinforcement phase (an SSE-film) exhibits compressive flexure properties/response, which cancels out the beneficial stiffness gain of the quasi-isotropic architecture. This is unique to the Tensylon 30A as the fiber-based HB210 system still demonstrates an improvement in peak BFD even with the Helical – 45/CP fiber architecture (see Fig. 11). The thinner Tensylon 30A film layers (two sublayer sheets, as illustrated in Fig. 1) may be micro-buckling (kink banding) under a flexural compressive loading without benefit of shear transfer given the matrix constituent is a weaker interlaminar coating between layers. This deformation may be observable under a fine-resolution XCT scan; however, the XCT scans performed for this study were expedient short scans meant to identify global deformation such as delamination, through-thickness impact dent, and global kinking or crumpling. The displacement contours at 50 and 70 J for Tensylon 30A are given in Figs. 13 and 14, respectively. From Fig. 12, the CP/Helical – 45 and the 100% Helical – 45 (quasi-isotropic) fiber architectures exhibit almost identical impact performance, suggesting that a minimum "loading" of [45°/135°] plies is sufficient to achieve the beneficial effect of reducing peak BFD for the stiffer SSE-film material system.

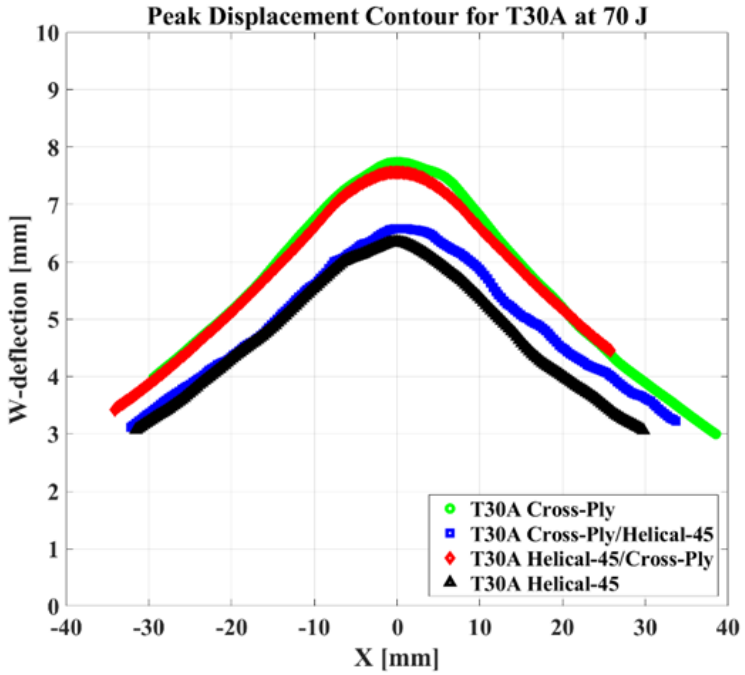

Fig. 14 Displacement contour at peak BFD for a 70-J impact energy for Du Pont HSBD Tensylon 30A

3.4 LVI Response of Honeywell SpectraShield 4232

The DIC results for the dynamic peak BFD for Honeywell SpectraShield 4232 are presented in Table 5 and Fig. 15. The SS-4232 material proved to be the stiffest UHMWPE fiber system tested in impact with very similar impact performance to Tensylon 30A. The stiffness of the SS-4232 material significantly affects its structural properties and response, especially in impact flexure. Due to limited material, sequencing effects were not investigated for the SS-4232 material (only one large panel was fabricated per fiber architecture) and no replicate impact tests were performed. From Table 5 and Fig. 15, the quasi-isotropic architecture, Helical – 45, posted a 13% and 15% reduction in the peak BFD over the reference CP architecture for 50- and 70-J impacts, respectively. Both impact energy levels saw an improvement in the peak BFD with the CP/Helical – 45 architecture of 6% and 12%, respectively. The improvement in peak BFD at the 70-J impact was almost identical between the CP/Helical – 45 and 100% Helical – 45 (quasi-isotropic) architectures, a trend also demonstrated for both the Tensylon 30A and HB210. The contours at peak BFD are given in Figs. 16 and 17 for SS-4232 and exhibit similar trends for a stiff UHMWPE material under impact. The three fiber architectures have a very similar performance at 50 J (posting a range of peak BFD of approximately 0.8 mm), again demonstrating that this impact energy may be too low to evaluate the impact response. At the higher impact energy of 70 J, the notable observation is the near overlap of the Helical – 45 and CP/Helical – 45 curves, demonstrating, like for the Tensylon 30A, that stiffer UHMWPE materials need only a smaller "loading" of quasi-isotropic architecture to achieve a significant improvement in the peak BFD over the reference CP lay-up.

Table 5 Peak dynamic BFD measured through DIC for Honeywell SpectraShield 4232 per fiber architecture for each impact energy

	Impact energy					
	25 J		50 J		70 J	
SpectraShield 4232	Peak δ (mm)	Impact efficiency	Peak δ (mm)	Impact efficiency	Peak δ (mm)	Impact efficiency
CP	4.2	0.25	5.7	0.29	7.1	0.30
CP/Helical – 45	N/A	N/A	5.3	0.24	6.2	0.28
Helical – 45	N/A	N/A	4.9	0.26	6.0	0.31

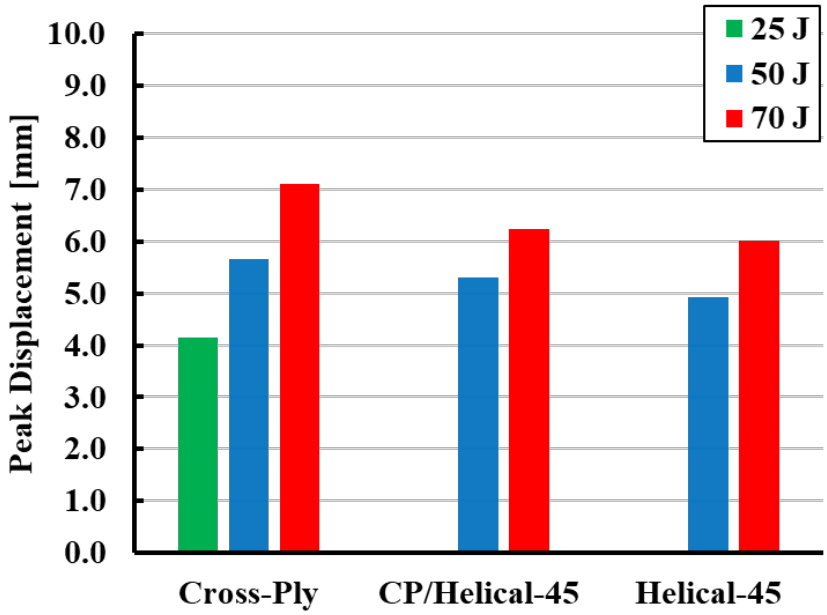

Fig. 15 Peak BFD for Honeywell SpectraShield 4232 for each fiber architecture at impact energies of 25, 50, and 70 J

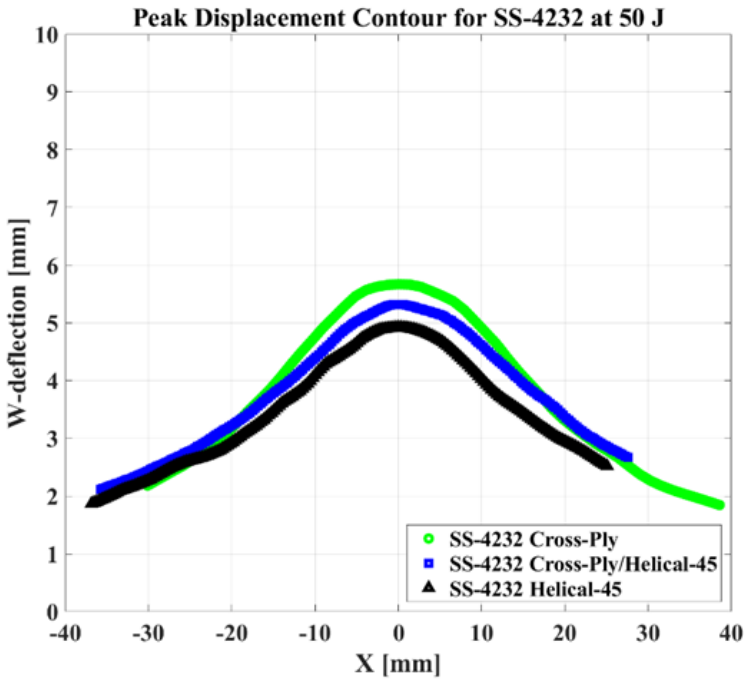

Fig. 16 Displacement contour at peak BFD for a 50-J impact energy for Honeywell SpectraShield 4232

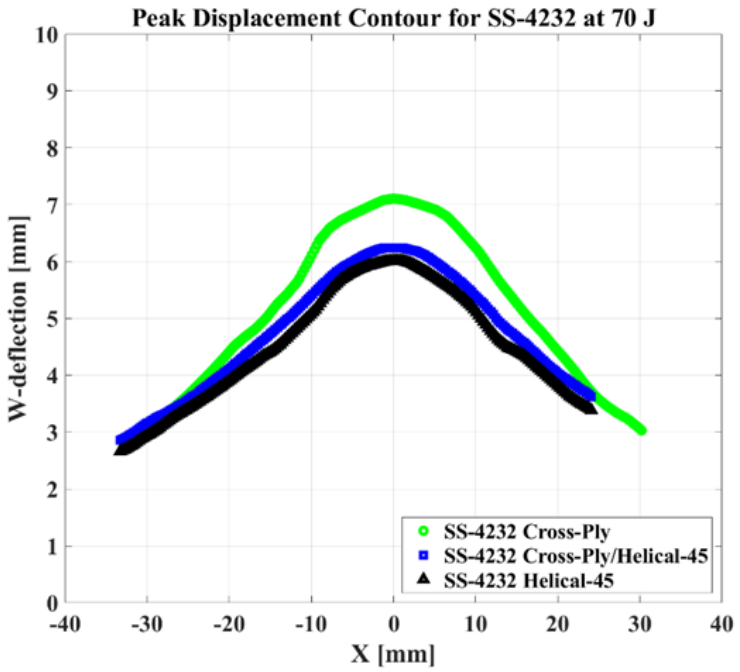

Fig. 17 Displacement contour at peak BFD for a 70-J impact energy for Honeywell SpectraShield 4232

3.5 Damage Analysis

The damage and deformation mechanisms were identified through two nondestructive visualization methods: visual inspection of the strike face with a through-thickness light source and XCT scanning and analysis of the 3-D volume. The high-definition images of the strike faces of each material are presented in Appendix B, Figs. B-1 (HB212), B-2 (HB210), B-3 (T30A), and B-4 (SS-4232). The XCT results are reduced to characteristic 2-D images of unique UHMWPE materials and visualizations of damage discovered in impacted UHMWPE samples. The interface between the CP and quasi-isotropic architectures is also visualized for any damage due to flexural impact. A general assessment of the dominant deformation and damage mechanics typically observed is presented for the quasi-isotropic Helical – 45 fiber architecture. The presented XCT scans were lower-resolution scans meant to visualize large-scale damage over length scales consistent with millimeters and centimeters, and cannot be used to visualize finer length scales as between fibers, fiber/matrix interfaces, and interlaminar planes. Lower-resolution scanning parameters were purposefully selected to reduce the burden of multiple lengthy scans on the CT technicians while providing sufficient information to determine dominant deformation and damage mechanisms.

The HB212 was the most compliant UHMWPE material investigated due to its rubber-based polymer matrix and was expected to demonstrate the most interesting

deformation mechanisms compared to the stiffer UHMWPE materials. Figures 18 and 19 give a variety of cross sections through a 50-J impact (Fig. 18) and 70-J impact (Fig. 19) HB212 sample with the CP/Helical – 45 fiber architecture. The dominant deformation mechanisms observed for HB212 were a large impact dent, "halo" delaminations through-thickness framing the impact site, a kink band crimp that roughly aligned with the [0°/90°] reinforcement directions, and a large delamination extending from the impact site clear through to the sample edge aligning with the interface between the CP and quasi-isotropic fiber architectures. The strike-face indent, which is pictured in both Figs. 18 and 19, is squared on the surface indent and transitions to a rounded "halo" of delaminations framing the impact site within. For the HB212 material, fiber tension pull-out due to the pull of the impact and compressive flexure of the strike face prominently occurs throughout the thickness but especially at the interface of the dissimilar fiber architectures and can be clearly seen in the figures in Appendix B (the strike-face images) and the more detailed XCT scans. More extensive delaminations of the same type are seen in Fig. 19 for the 70-J impact, although caution must be exercised when distinguishing artifacts due to threshold grayscaling of the XCT data versus actual damage.

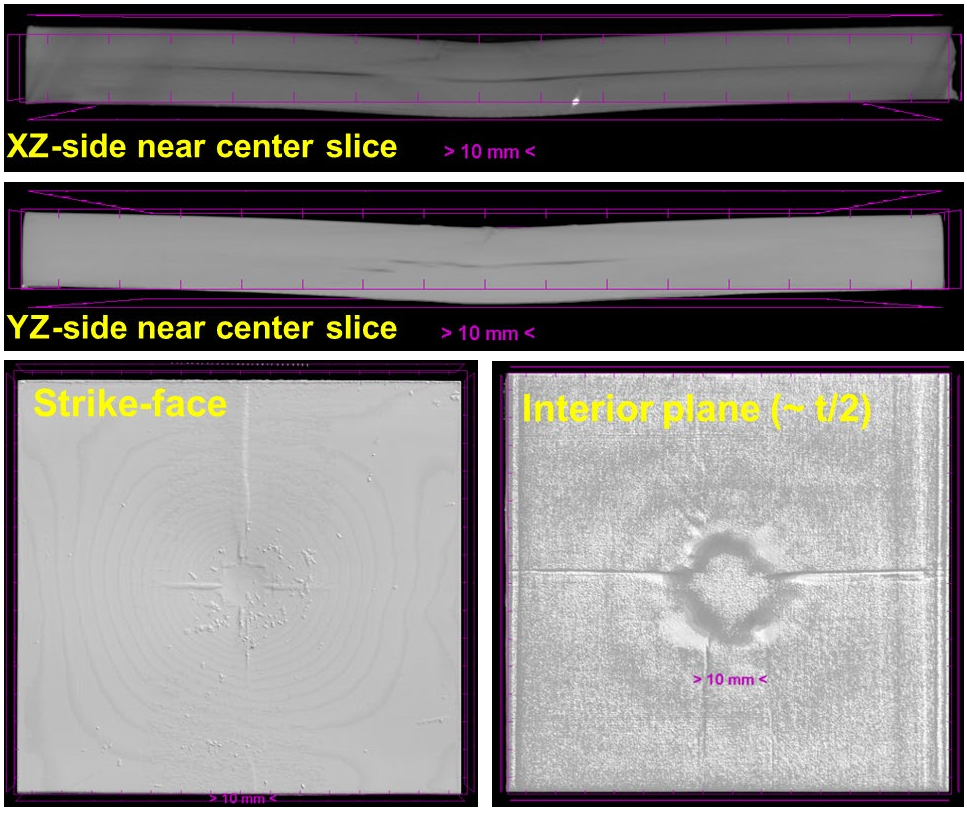

Fig. 18 Through-thickness (t) deformation and damage for a 50-J impact for sample 2201A-2 of DSM Dyneema HB212 with the CP/Helical – 45 fiber architecture. Imaging generated using Bruker CT-Vox visualization software.

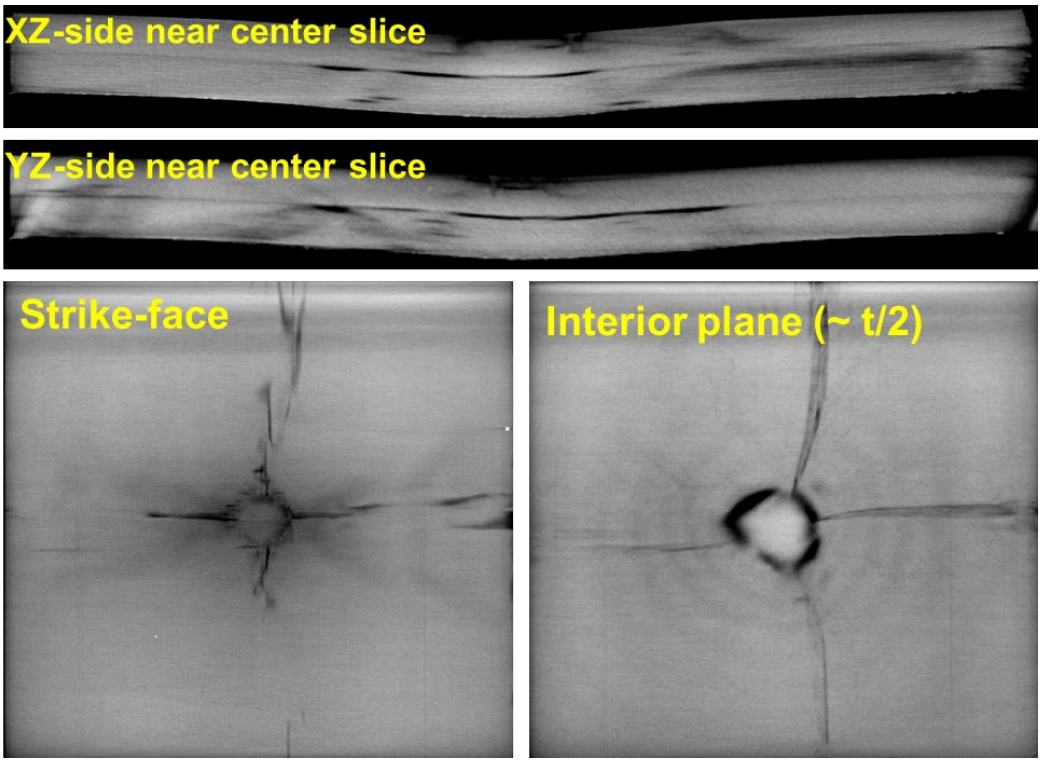

Fig. 19 Through-thickness (t) deformation and damage for a 70-J impact for sample 2201A-3 of DSM Dyneema HB212 with the CP/Helical – 45 fiber architecture. Imaging generated using 3DSlicer.

An important aspect of this research is to evaluate the effect of sequencing different fiber architectures on the impact response. Manipulating fiber architectures so that both the CP and quasi-isotropic architectures in turn are configured on the strike face under an impact demonstrated that there was a weak effect on the impact response for the stiffer UHMWPE materials, but statistically no effect for the more compliant HB212. What observable deformation and damage mechanisms are apparent when a stiffer quasi-isotropic fiber architecture is situated on the strike face versus the back face given that both configurations undergo global flexural compression versus tension, respectively? Figures 20 and 21 give near-center XCT visualizations of the transition interface at the impact site between CP and Helical – 45 fiber architectures, where the CP architecture is on the strike face (Fig. 20) and the Helical – 45 architecture is on the strike face (Fig. 21). Both figures represent visualization for all studied materials at the highest impact energy of 70 J to increase the chance of observing the most distinct types of damage. Unfortunately, Fig. 21 is compromised because no corresponding Helical – 45/CP fiber architecture was impacted at 70 J for Honeywell SS-4232 and the scan for the Tensylon 30A was not performed.

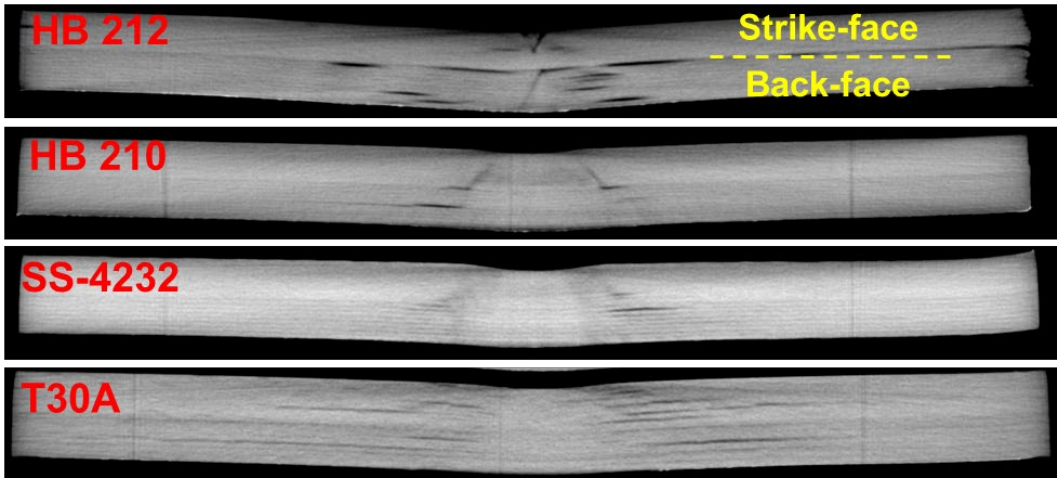

Fig. 20 Through-thickness deformation and damage for all UHMWPE material investigated with a CP/Helical – 45 fiber architecture at 70-J impact. Imaging generated using 3DSlicer visualization software.

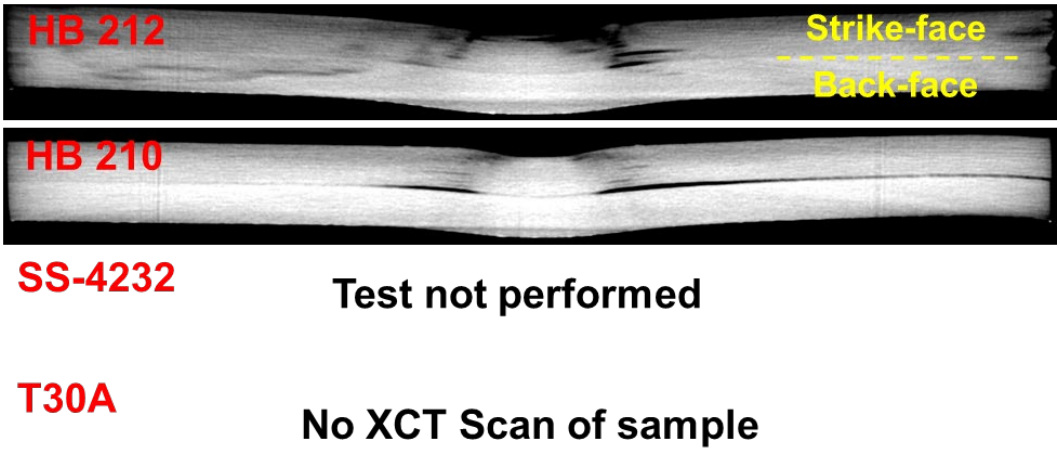

Fig. 21 Through-thickness deformation and damage for all UHMWPE material investigated with a Helical – 45/CP fiber architecture at 70-J impact. Imaging generated using 3DSlicer visualization software.

Figure 20 presents the characteristic damage observed for a 70-J impact for the fiber architecture configuration that posted the lower peak BFDs (the CP/Helical – 45 architecture). Two of the fiber systems, the DSM HB210 and Honeywell SS-4232, illustrate a cone-shaped damage volume through-thickness under the impact site with accompanying isolated interlaminar branching delaminations. Tensylon 30A, the lone SSE-film system, has a less-defined cone damage volume but many more interlaminar delaminations through-thickness, suggesting that the dominant deformation (energy dissipation) mechanism for the film-based Tensylon 30A under impact is interlaminar delamination. Except for the HB212, the CP/Helical – 45 architecture samples are not exhibiting any preferred damage at the orthogonal interface (transition from light to dark gray in the figure) between

the CP and quasi-isotropic architecture in Fig. 20. The opposite is illustrated in Fig. 21 for the Helical – 45/CP fiber architecture, at least for the DSM HB210 material, as a prominent delamination has opened at the interface between the two architectures. One of the reasons a 50%/50% split in fiber architectures was chosen for the impact samples in this study is that the interface between the two fiber architectures would approximately correspond to the neutral axis in bending with maximum bending stress and zero shear stress. This observed damage in this single sample may be unique or it may be an interplay of two fiber architectures (CP vs. quasi-isotropic), which respond differently under flexural compression and tension and create a discontinuity at the interface that is under maximum bending stress and manifests as a global delamination. Here, the stiffer quasi-isotropic architecture may be kinking under compression (when it is configured on the strike face), adding to the discontinuity at the interface and contributing to a larger-scale delamination. Unfortunately, the scans for the two stiffest materials, SS-4232 and Tensylon 30A, are not available to evaluate this conjecture.

The last XCT data comparison is given in Fig. 22 and presents the near-center cross sections for all UHMWPE materials investigated at an impact of 70 J for the 100% Helical – 45 (quasi-isotropic with N = 2 periodicity) fiber architecture. This architecture is consistent through-thickness and no interface issue is expected. Unfortunately, corresponding XCT scans of the CP architecture are not available due to the selected ultrasonic scanning methodology presented in Boyd.[6] The 100% Helical – 45 fiber architecture posted the lowest dynamic peak BFDs of all the fiber architectures investigated. From Fig. 22, the compliant HB212 material exhibits the lowest internal damage with a cone shape through-thickness and a few “halo” delaminations about the impact site. The remaining UHMWPE materials all demonstrate extensive “halo” delaminations about the impact site with the two stiffest materials, SS-4232 and Tensylon 30A, having the most. For stiffer UHMWPE material systems regardless of fiber/matrix or SSE-film, the dominant energy dissipation mechanism under impact is delamination about the impact cone.

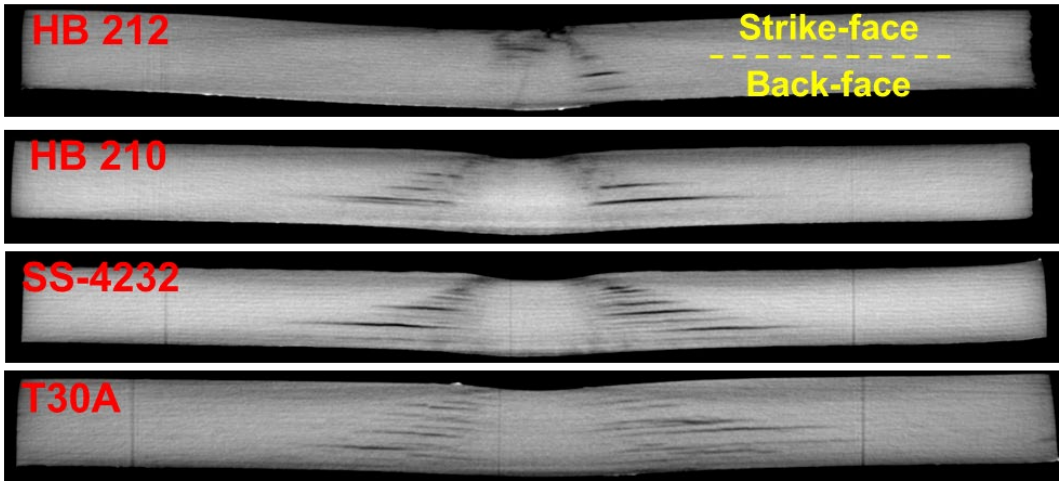

Fig. 22 Through-thickness deformation and damage for all UHMWPE material investigated with a Helical – 45 fiber architecture at 70-J impact. Imaging generated using 3DSlicer visualization software.

3.6 Discussion: Fiber Architecture in Helmet Shells

The effect of fiber architectures on impact response at two different impact energies were evaluated for four ballistic-grade UHMWPE materials of interest for insertion into personnel protection systems. This work was motivated by previous investigations at the DEVCOM Army Research Laboratory (ARL) conducted by Vargas-Gonzalez et al.,[9] which proposed a unique fiber architecture called ARL X-hybrid, which demonstrated up to a 40% reduction in dynamic peak BFD while maintaining the RTP V_{50} performance to within 90% of the reference 100% CP fiber architecture. The ARL X-hybrid architecture displaced a few cross-plied ([0°/90°]) sheets by rotating (indexing) the commercially cross-plied ballistic-grade UHMWPE sheets by a bias off-axis angle with a rotation periodicity. The indexed angled sheets were configured toward the back-face portion of the ballistic impact sample presumably by design to maintain the RTP performance of the ARL X-hybrid architecture panel (the [0°/90°] CP fiber architecture (know through years of ballistic evaluation to post the best RTP V_{50} results). Displacing as few [0°/90°] layers as possible with [(0° + θ)/(90° + θ)] layers in the lay-up helped maintain the ballistic impact performance while the improved flexural rigidity of the quasi-isotropic architecture toward the back face significantly reduced the dynamic peak BFD. This strategy of introducing bias angle plies through indexing to the laminate lay-up is the key to designing fiber architecture configurations which enter a trade space of reducing BFD while maintaining RTP and enabling improved personnel protection systems with comprehensive impact performance (LVI to ballistic regime impact).

The LVI evaluation presented in this report demonstrated the same trend that incorporating a fractional percentage of quasi-isotropic architecture into the laminate lay-up reduces the dynamic peak BFD and improves the LVI performance for most UHMWPE materials. The impact performance of three different fiber architectures was evaluated using a flat plate LVI methodology,[6] which was developed to correlate directly to blunt (low-velocity) impact of combat helmet shells. Helmet shells are complex double curvature systems, manufactured through thermoforming initially flat, cross-plied UHMWPE material constituents, which are required to demonstrate a high degree of in-plane shearing to achieve the double curvature shape of the helmet shell without excessive wrinkling or tearing. Thermoforming produces a final fiber architecture configuration, which preserves circumferentially the initial cross-plied architecture and generates regions of highly sheared architectures. A combination of cross-ply and angled fiber architectures could be generated through-thickness around the circumference of the shell with certain "hybrid" designs. Evaluation of the blunt impact performance of these "hybrid" architectures and their sequencing effects is critically important to understanding how indexed fiber architecture designs can be incorporated into the helmet shell to mitigate peak BFD (as there are tight tolerance offsets between the shell and the head).

4. Conclusions

A flat plate LVI performance evaluation was conducted on four commercially available ballistic-grade UHMWPE materials with three different fiber architectures suggested by prior ballistic testing at ARL (Vargas-Gonzalez et al.[9]) and architecture configurations representative of those encountered in thermoformed complex double curvature structures. The four UHMWPE materials encompass a wide range of ballistic-grade materials to represent both fiber and film systems and compliant and stiff matrix binder materials. The three fiber architectures consisted of the reference (baseline) CP architecture, a Helical – 45 architecture (fully quasi-isotropic architecture with a periodicity of 2), and a 50%/50% combination of the two. The impact samples were evaluated at two impact energies, 50 and 70 J, which directly correlate to prescribed impact velocities defined under blunt impact conditions for combat helmets. The key screening metrics include dynamic peak BFD, displacement contour at peak, and residual dent. The deformation and damage mechanisms per material per fiber architecture were also evaluated to identify the dominant mode of damage.

The 100% Helical – 45 architecture consistently posted the lowest peak BFDs for all four UHMWPE materials investigated, but demonstrated an increase in through-thickness "halo" delaminations about the central impact cone-shaped dent.

However, for the stiffer UHMWPE materials including HB210, SS-4232, and Tensylon 30A there was little difference between the impact BFD of the CP/Helical – 45 and Helical – 45 architectures to justify the extra [45°/135°] plies at the lowest impact energy of 50 J. The most compliant UHMWPE material, DSM Dyneema HB212, benefitted the most from the addition of indexed orthogonal fiber architectures posting a 44% decrease in peak BFD (Table 2 and Figs. 6 and 7) and reduced presence of internal damage (Fig. 22, top) for the Helical – 45 architecture. Sequence effects as represented by the CP/Helical – 45 and Helical – 45/CP architectures had a negligible effect on peak BFD for the compliant HB212 material and were statistically indifferent for the three stiffer UHMWPE materials. However, the 70-J impact energy suggested that, for the three stiffer materials, configuring the quasi-isotropic (Helical – 45) architecture on the back face led to a reduced peak BFD approaching the 100% Helical – 45 performance. This possibly suggests that placing or "front loading" the more-compliant CP fiber architecture on the strike face (flexural compression) takes advantage of the stiffer quasi-isotropic fiber architecture on the back face (flexural tension) and results in a stiffer panel under impact and lower BFD. The interface (transition) between the CP and Helical – 45 fiber architecture is expected to be more susceptible to global delamination (especially with the Helical – 45/CP architecture); however, limited XCT data for SS-4232 and Tensylon 30A inhibited a full evaluation of the interface except for HB212 and HB210, which both showed delaminations at 50 J (HB212) and 70 J (HB210), although both samples stayed together.

5. References

1. National Research Council. Review of Department of Defense test protocols for combat helmets. The National Academies Press; 2014.

2. Defense Veterans Brain Injury Center. Traumatic brain injury fact sheet. Armed Forces Health Surveillance Center; 2018.

3. Brown AD, Matheis EA, Rafaels KA. Experimental evaluation of behind-helmet blunt trauma ballistic impacts. DEVCOM Army Research Laboratory (US); 2021 Sep. Report No.: ARL-TR-9314.

4. Matheis EA, Wozniak SL, Loftis KL, Rafaels KA. Injury outcomes of behind helmet blunt trauma impacts. DEVCOM Army Research Laboratory (US); 2021 Jun. Report No.: ARL-TR-9169.

5. Wozniak SL, Matheis EA, Brown AD, Goertz AR, Loftis KL, Kulaga AR, Jubb KM, Gillich PJ, Rafaels KA. A method for studying the biomechanics of behind-helmet blunt trauma (BHBT). DEVCOM Army Research Laboratory (US); 2022 Feb. Report No.: ARL-TR-9407.

6. Boyd SE. A flat-plate low-velocity impact methodology to evaluate ultra-high-molecular-weight polyethylene (UHMWPE) ballistic materials for head protection systems. DEVCOM Army Research Laboratory (US); 2021 Aug. Report No.: ARL-TR-9276.

7. Vargas-Gonzalez LR. Ballistic modification of ultra-high molecular weight polyethylene composites through processing. Proceedings of the SAMPE 2015 Conference; 2015.

8. Vargas-Gonzalez LR, Gurganus JC. Hybridized composite architecture for mitigation of non-penetrating ballistic trauma. Int J Impact Eng. 2015;86:295–306.

9. Vargas-Gonzalez LR. Analysis of ARL X hybrid impact behavior with varying angle offset. Conference Proceeding, CAMX 2015; 2015 Oct 26–29.

10. Hazard MK, Hallett S, Curtis PT, Iannucci L, Trask RS. Effect of fibre orientation on the low velocity impact response of thin Dyneema® composite laminates. Int J Impact Eng. 2017;100:35–45.

11. Staniszewski JM, Boyd SE, Bogetti TA. A multi-scale modeling approach for UHMWPE composite laminates with application to low-velocity impact loading. Int J Impact Eng. 2022;159:104031.

12. Karthikeyan K, Kazemahvazi S, Russell BP. Optimal fibre architecture of soft-matrix ballistic laminates. Int J Impact Eng. 2016;88:227-237.

13. Boyd SE, Plaisted TA. A low-velocity impact methodology for assessing durability and blunt impact performance of ultra-high-molecular-weight polyethylene (UHMWPE) helmet shells. CCDC Army Research Laboratory (US); 2019 Nov. Report No.: ARL-TR-8850.

14. Boyd SE, Plaisted TA, Staniszewski JM. A low-velocity impact methodology for assessing durability and blunt impact performance of ultra-high-molecular-weight polyethylene (UHMWPE) helmet shells – Part II: deformation and damage analysis. DEVCOM Army Research Laboratory (US); 2020 Sep. Report No.: ARL-TR-9042.

Appendix A. Periodicity of Indexing

Ply #	Periodicity $n = 1$	$n = 2$	$n = 2$	
	Strike-Face			
1	[0/90]	[0/90]	[45/135]	
2	[45/135]	[0/90]	[45/135]	
3	[0/90]	[45/135]	[0/90]	
4	[45/135]	[45/135]	[0/90]	
5	[0/90]	[0/90]	[45/135]	
6	[45/135]	[0/90]	[45/135]	
7	[0/90]	[45/135]	[0/90]	
8	[45/135]	[45/135]	[0/90]	
9	[0/90]	[0/90]	[45/135]	
10	[45/135]	[0/90]	[45/135]	Mid-Plane
11	[0/90]	[45/135]	[0/90]	
12	[45/135]	[45/135]	[0/90]	
13	[0/90]	[0/90]	[45/135]	
14	[45/135]	[0/90]	[45/135]	
15	[0/90]	[45/135]	[0/90]	
16	[45/135]	[45/135]	[0/90]	
17	[0/90]	[0/90]	[45/135]	
18	[45/135]	[0/90]	[45/135]	
19	[0/90]	[45/135]	[0/90]	
20	[45/135]	[45/135]	[0/90]	
	Back-Face			

Fig. A-1 The effect of periodicity on indexing initially cross-plied ultra-high-molecular-weight polyethylene (UHMWPE) feedstock sheets by 45° using a hypothetical 20-ply laminate. Column A (n =1) gives an alternating configuration with no particular architecture favored on the strike face vs. the back face. Columns B and C illustrate a periodicity of n = 2. Starting the lay-up with an indexed vs. cross-ply layer/sheet will either "front-load" (column B) or "back load" (column C) the laminate with cross-plied layers and effect the impact performance.

Appendix B. Visualization of Strike Face

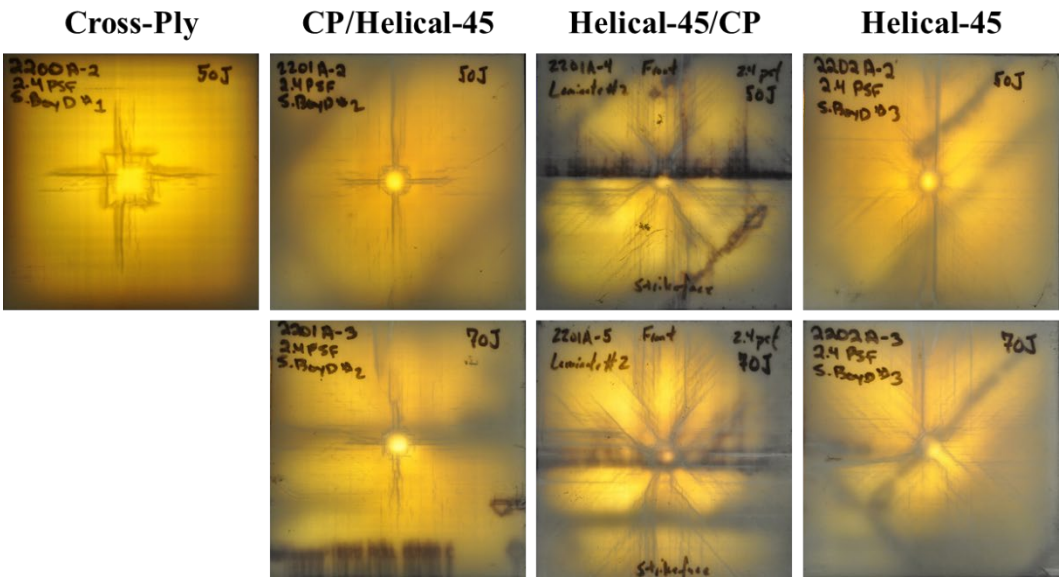

Fig. B-1 High-definition imaging of the impact strike-face damage using through-thickness light source for DSM Dyneema HB212. The panel IDs and impact energies are written on the sample face.

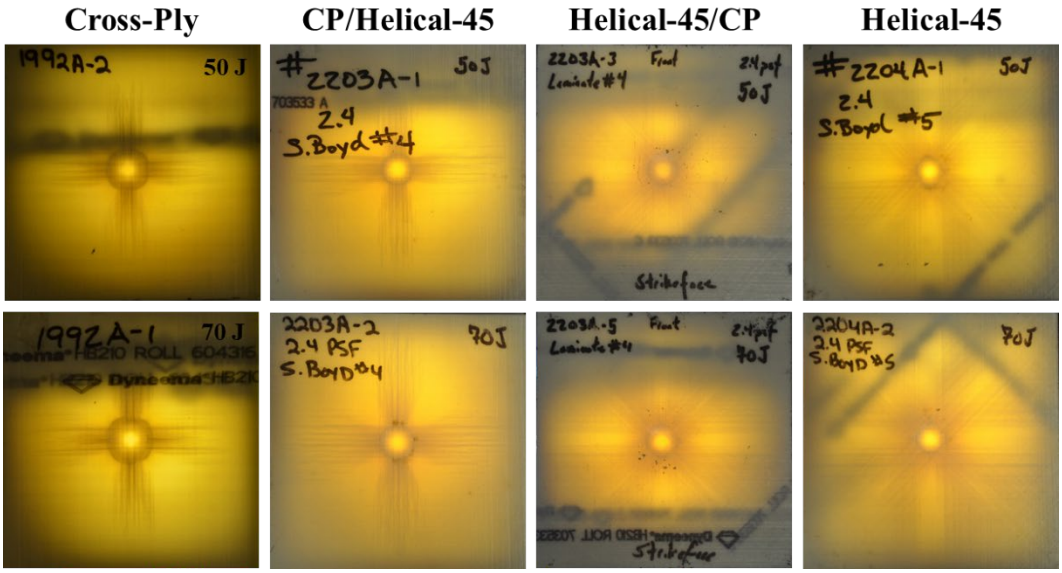

Fig. B-2 High-definition imaging of the impact strike-face damage using through-thickness light source for DSM Dyneema HB210. The panel IDs and impact energies are written on the sample face.

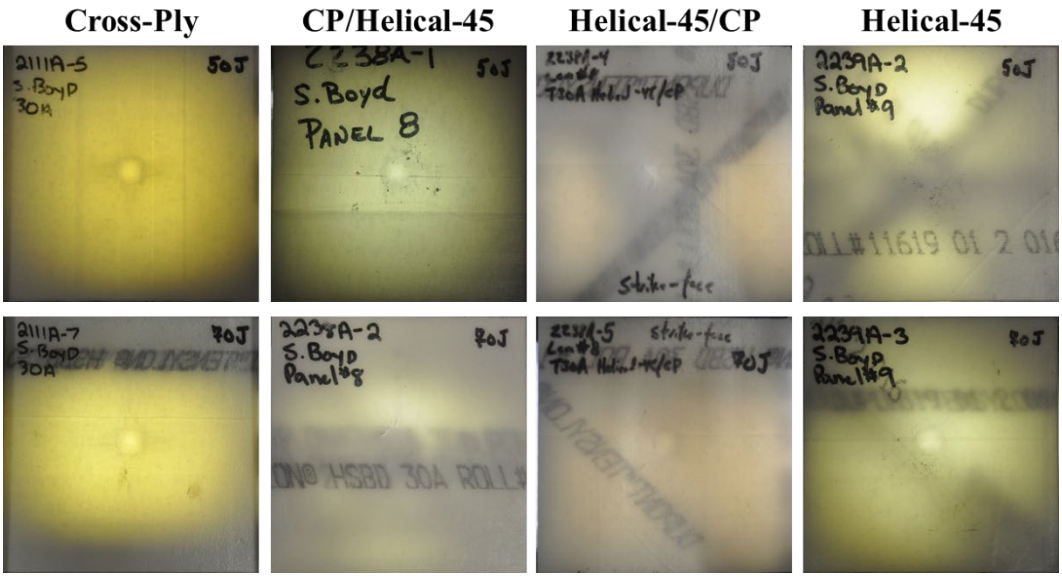

Fig. B-3 High-definition imaging of the impact strike-face damage using through-thickness light source for Du Pont Tensylon 30A. The panel IDs and impact energies are written on the sample face.

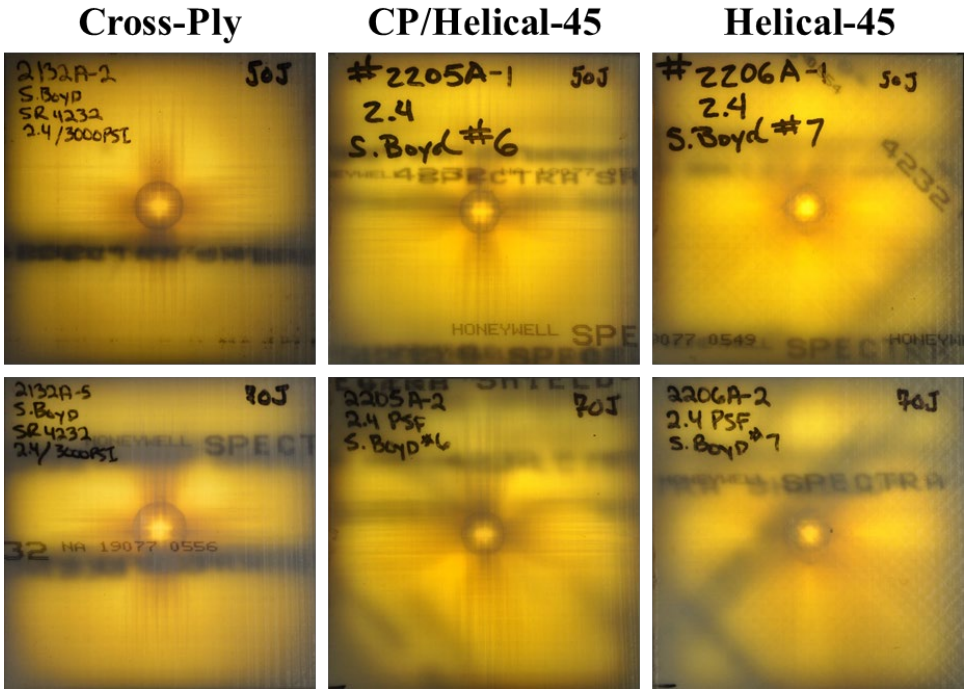

Fig. B-4 High-definition imaging of the impact strike-face damage using through-thickness light source for Honeywell SpectraShield 4232. The panel IDs and impact energies are written on the sample face.

List of Symbols, Abbreviations, and Acronyms

2-D	two-dimensional
3-D	three-dimensional
AD	areal density
ARL	Army Research Laboratory
ASTM	American Society of Testing and Materials
BABT	behind-armor blunt trauma
BFD	back-face deflection/displacement
BHBT	behind-helmet blunt trauma
CP	cross-ply fiber architecture (orthogonal [0°/90°])
CT	computed tomography
DEVCOM	US Army Combat Capabilities Development Command
DIC	digital image correlation
ID	identification
LVI	low-velocity impact
n	periodicity of rotation frequency
N/A	not applicable
PD	purchase description
PE	polyethylene
PU	polyurethane
RTP	resistance to penetration (referring to the ballistic testing standard)
SoTA	state of the art
SS	SpectraShield
SSE	solid-state extruded
UHMWPE	ultra-high-molecular-weight polyethylene

V_{50}	ballistic limiting velocity; velocity at which a specific projectile (threat) is expected to penetrate the armor half of the time
XCT	X-ray computed tomography

1 (PDF) DEFENSE TECHNICAL INFORMATION CTR
DTIC OCA

1 (PDF) DEVCOM ARL
FCDD RLD DCI
TECH LIB

3 (PDF) PROG EXECUTIVE SOLDIER OFC
AL DE GROOT
JA HOPPING
T SMITH
BN SUNDBERG

13 (PDF) DEVCOM SOLDIER CENTER
RV DILALLA
JC PARKER
D KUBIAK
CA HEWITT
WS SHAW
SA BENNETT
JA ORLANDO
DM OTTERSON
BP FASEL
MJ ROTH
DS COLANTO
JA KIREJCZYK
MA MAFFEO

17 (PDF) DEVCOM ARL
FCDD RLW B
LR VARGAS-GONZALEZ
CP HOPPEL
RC BECKER
AL TONGE
PJ GILLICH
FCDD RLW MA
JM STANISZEWSKI
SE BOYD
M YEAGER
TA BOGETTI
TA PLAISTED
ED WETZEL
FCDD RLW MB
DJ O'BRIEN
FCDD RLW TB
SS SATAPATHY
TG ZHANG
M KLEINBERGER
FCDD RLW TF
PA JANNOTTI
CS MEYER